

Please cite the Published Version

Shi, X, Chen, J, Beake, BD, Liskiewicz, TW and Wang, Z (2021) Dynamic contact behavior of graphite-like carbon films on ductile substrate under nano/micro-scale impact. *Surface and Coatings Technology*, 422. ISSN 0257-8972

DOI: <https://doi.org/10.1016/j.surfcoat.2021.127515>

Publisher: Elsevier

Version: Accepted Version

Downloaded from: <https://e-space.mmu.ac.uk/628191/>

Usage rights:  [Creative Commons: Attribution-Noncommercial-No Derivative Works 4.0](https://creativecommons.org/licenses/by-nc-nd/4.0/)

Additional Information: This is an Author Accepted Manuscript of an article published in *Surface and Coatings Technology*.

Enquiries:

If you have questions about this document, contact openresearch@mmu.ac.uk. Please include the URL of the record in e-space. If you believe that your, or a third party's rights have been compromised through this document please see our Take Down policy (available from <https://www.mmu.ac.uk/library/using-the-library/policies-and-guidelines>)

Dynamic contact behavior of graphite-like carbon films on ductile substrate under nano/micro-scale impact

Xiangru Shi^{a*}, Jian Chen^{b*}, Ben D. Beake^c, Tomasz W. Liskiewicz^d, Zehua Wang^a

a. College of Mechanics and Materials, Hohai University, Nanjing 210098, China

b. School of Materials Science and Engineering, Jiangsu Key Laboratory for Advanced Metallic Materials, Southeast University, Nanjing 211189, China

c. Micro Materials Ltd., Willow House, Yale Business Village, Ellice Way, Wrexham, LL13 7YL, UK

d. Faculty of Science and Engineering, Manchester Metropolitan University, John Dalton Building, Charles Street, Manchester M15 6BH, UK

* Corresponding author. E-mail address: sxr12009210@163.com (Xiangru Shi), j.chen@seu.edu.cn (Jian Chen)

Abstract

Coated components are often subjected to high strain rate and repetitive contact damage in practical service, so how to quickly evaluate the dynamic contact behavior of the thin protective coating is particularly important. Highly resolved single nano-impact and novel multiple micro-scale impact tests were used to investigate the dynamic hardness and fatigue failure of 0.55-1.52 μm thick graphite-like carbon (GLC) films on 316L stainless steel with varied thickness, respectively. By analyzing the impact depth and velocity before and after the indenter first contact with the sample, the dynamic hardness of GLC film/substrate system was obtained reasonably based on the energy approach in single nano-impact tests. Possible reasons for the higher dynamic hardness than quasi-static hardness include overestimation of the plastic absorbed energy W_p and the strain rate sensitivity of materials. The thickest film/substrate system studied had a higher dynamic hardness than the thinner films due to its higher load carrying capability. Results with the multiple micro-impact technique showed that a GLC film with intermediate thickness (1.1 μm) was more resistant to the impact fatigue, while the thinnest film, 0.55 μm , exhibited more pronounced radial cracks under the indent and the thickest film, 1.52 μm , showed more significant edge ring cracks, these differences resulting from the combined action of stress distribution, film microstructure and mechanical properties.

Keywords: single nano-impact, multiple micro-impact, dynamic hardness, fatigue failure

1. Introduction

Graphite-like carbon films (GLC) are amorphous carbon thin films composed of significant sp^2 -hybridized carbon atoms cross-linked by a small amount of sp^3 bonds. Due to their outstanding properties of high mechanical strength, excellent tribological behavior, desirable chemical inertness and bio-comparability, GLC films have shown great potential in the fields of materials science, mechanical engineering and biomedical applications [1-4]. The performance of GLC films in many of these applications is limited by their resistance to contact damage, and numerous studies have been conducted by using the indentation tests, scratch tests, and pin-on-disk wear tests with varied indenters, loads and environments [5-9]. However, the film/substrate system often experience more complex loading condition in practical applications, where the hard coatings are easily damaged by repetitive and high-strain-rate impact or impact-sliding [10-12]. Since the mechanical properties of materials often show the strain rate sensitivity, it is difficult to predict the deformation and failure mechanism of thin films at high strain rate from the quasi-static mechanical properties [13], emphasizing the importance of obtaining dynamic mechanical properties and failure mechanisms of thin films under impact conditions.

Improved understanding of the dynamic contact behavior of thin films is possible by nano-impact technology, which utilises pendulum-based loading to acquire the instantaneous dynamic response at the material surface with strain rates several orders of magnitude higher than in quasi-static indentation (Fig. 1a) [14,15]. Two different approaches can be carried out in the nano-impact test, which are known as the 'Multiple Impulse' and 'Dynamic Hardness' modules, respectively. The former can provide much closer simulation of actual service environment of materials under highly loaded intermittent contact by performing repetitive impact at a particular location, and evaluate the behavior of impact wear, adhesive failure and fatigue fracture qualitatively by recoding the evolution of impact depth-time curves in real time (Fig. 1b) [16-18]. In general, a single rapid increase in penetration depth may represent the adhesive failure of the coatings, and a series of several smaller jumps in the penetration depths corresponds to a more gradual cohesive failure. The latter approach when combined with a high data acquisition rate system can observe the entire mechanical response of single nano-impact curve, and calculate the dynamic mechanical properties such as dynamic hardness and dynamic toughness quantitatively by analyzing the energy dissipation of impact indenter before and after entering the sample (Fig. 1c) [19-21]. The initial impact energy of both approaches can be adjusted by changing the impact distance, applied load and the effective mass of the pendulum.

In practice, the majority of studies using repetitive nano-impact testing have investigated the resistance of impact fatigue and failure mechanism of a wide range of coatings such as amorphous carbon, ceramics, polymers and other hard tool coatings

[14,18,22,23]. Beake et al. [24,25] pioneered this technique and summarized the damage evolution of tetrahedral amorphous carbon films on silicon substrate with a blunt Berkovich indenter. Chen et al. [26] investigated the dynamic loading behavior of TiN-based coatings by using repetitive nano-impact with a blunt cube corner diamond probe. It was found the failure mechanism under dynamic loading is obviously different from that under quasi-static condition, in which the generation of cracks tends to be transverse and the failure of the films is cohesive failure. Wheeler and Gunner [10] proposed the impact fatigue failure map to describe the damage evolution of a sol-gel coating on repetitive contact with a sphero-conical diamond indenter. It is worth noting that a higher aspect ratio, sharp indenter (e.g. cube corner indenter) is often chosen as the test probe in these studies, aiming to induce fracture easily within a short time at high contact strain. On very hard materials there is a risk of eventual damage to the diamond indenter tip which increases the requirement to periodically monitor probe sharpness, potentially complicating the testing. A new developed micro-impact test proposed a solution to use blunter probe geometries in combination with higher forces. The micro-impact test increases the maximum applied loads to micro-range of 0.5~5 N and the initial impact energy to 2 orders of magnitude greater than the maximum possible in the nano-impact technique, while retaining the intrinsic depth sensing capability of the nano-impact test [27].

Compared to the repetitive nano-impact testing, the investigation on the high-precision single impact with 'Dynamic Hardness' module to obtain quantitative information of dynamic mechanical properties is less well developed. Based on the one-dimensional contact model by Andrews et al [28], Constantinides and his co-workers [21] investigated the impact response of Al (1100) at different contact velocities by using single impact testing with nanoscale spatial, force and temporal resolution. The obtained dynamic hardness of Al is about 0.29 GPa, a little higher than the quasi-static hardness of 0.27 GPa. Somekawa and Schuh [29] found there is a good linear relationship between the obtained dynamic hardness and quasi-static hardness with a wide range of strain rates from 10^{-3} /s to 150 /s by investigating the high-strain-rate contact behavior of fine-grained magnesium alloys. Ghosh et al. [20] observed that the nano-impact hardness of three different materials displayed a decreasing trend with increasing indentation depth, i.e. a dynamic size effect that is similar to the indentation size effect under quasi-static conditions. In our previous study [30], single crystal Al (110) was chosen to investigate the dynamic hardness based on the common energy approach and Meyer's hardness method, respectively. The single-impact studies described above were all on bulk materials, and there are very few reports focusing on the dynamic mechanical properties of thin films or film/substrate system.

Therefore in this study, three different thickness GLC films deposited on 316L stainless steel were chosen to investigate the dynamic hardness and impact fatigue resistance by using the single nano-impact and repetitive micro-impact testing,

respectively. The main aims of this work were (i) to provide an energy-based method to evaluate the dynamic mechanical properties of thin films or film/substrate system, (ii) improve the understanding of impact fatigue failure of hard coatings deposited on ductile substrates by using the novel micro-impact test, (iii) discuss the influence of film thickness on their dynamic contact behavior. Although the study here is GLC on 316L stainless steel, this approach can be applied to any film/substrate system.

2. Experimental Section

2.1. Film preparation

The GLC films with thickness of 0.55 μm , 1.10 μm and 1.52 μm (hereafter referred to as GLC-1, GLC-2 and GLC-3, respectively) were deposited on 316L stainless steel and single crystal Si substrates by using closed field unbalanced magnetron sputtering system (UDP-650/4, Teer Coating Ltd., UK) as described previously [31]. Prior to deposition, the substrate was cleaned ultrasonically in acetone and ethanol for 20 min in succession, and then hanged in the chamber equipped with two Ti targets and two graphite targets opposing each other. When deposition begun, an adhesion promoting Ti layer of 0.2 μm was firstly deposited on the substrate. After that, a Ti-C gradient layer was produced by decreasing the Ti target currents and increasing the graphite target currents gradually, and finally the deposition parameters remained unchanged to prepare the uniform GLC films with different sputtering time. The thicknesses of GLC films were measured from cross-sections with scanning electron microscopy (SEM). The surface morphologies and roughness was determined by atomic force microscopy (AFM), and the bonding structure was investigated by Raman spectra and X-ray diffraction (XRD). The detailed characterization methodology is reported elsewhere [31].

2.2. Mechanical characterization

A NanoTest Vantage system (Micro Materials Ltd., Wrexham, UK) with low (0-500 mN) and high (0-30 N) load heads was used to perform the nano/micro-scale mechanical characterization. The instrument was calibrated on a fused silica reference sample following the procedure outlined in ISO14577 [32]. All tests were carried out in controlled environment (25 °C and 65% RH humidity).

2.2.1 Nanoindentation

The quasi-static nanoindentation tests were carried out with a Berkovich diamond indenter to compare with dynamic nano-impact. The peak indentation loads of 2-100 mN were set to clarify the substrate effect and indentation size effect over a wide depth range. The loading and unloading time was set to 20 s for all the testing conditions. The hold time at peak force was 10 s. The tests at each load were repeated 15 times at different locations to mitigate the influence of surface roughness. The quasi-static hardness (H_s) were obtained by power-law fitting (Oliver and Pharr

analysis) of unloading curves.

2.2.2 Single nano-impact

Single nano-impact tests with a spheroconical diamond indenter of 5 μm end radius were performed using the ‘Dynamic Hardness’ option of the impact module of the NanoTest system. As can be seen from Fig 1a, the nano-impact configuration utilises a specially designed solenoid fixed on the worktable and a ferromagnetic bead on the bottom of the pendulum. The indenter can be positioned at a set acceleration distance away from the sample surface, held by the solenoid connected to a timed relay [30]. Once the solenoid is activated, the indenter is released and accelerated towards the sample surface, and then instantaneous depth change as a function of time is recorded by a sensor with high rate data acquisition (Fig 1c). The initial impact energy can be controlled by varying the acceleration distance and/or force. In this study the acceleration distance was set to 15 μm , and the acceleration force was varied from 2-40 mN to obtain a range of impact energies. Five repeated tests were conducted at different positions for each load. The residual impression after nano-impact testing was characterized by AFM imaging (Bruker Co., Germany).

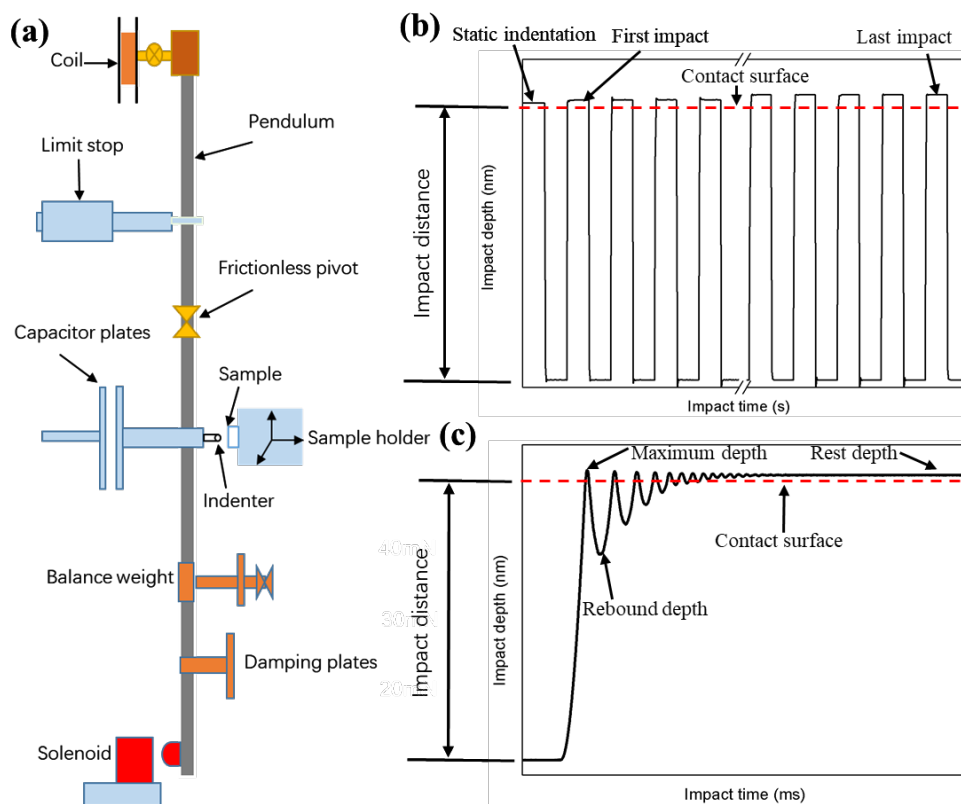


Fig. 1 (a) Schematic illustration of the NanoTest system showing the pendulum configuration for impact test, (b) typical impact depth-time curves of ‘Multiple Impulse’ mode, and (c) typical impact depth-time curves of ‘Dynamic Hardness’ mode.

2.2.3 Multiple micro-impact

The multiple micro-impact tests were conducted using the ‘Multiple Impulse’ module of NanoTest system with a high load head of 0-30 N. A spherical diamond indenter with end radius 40 μm was accelerated from a distance of 40 μm to generate repetitive impacts on the surface of GLC films. The applied acceleration force was varied between 0.1 N, 0.5 N, 1 N, 1.5 N and 2 N. Each impact cycle was complete in 4 s including 2 s load on and 2 s load off time intervals. The total time of each test was 300 s corresponding to 75 repetitive impacts at each location. There were three repeat tests at each load, spaced 200 μm apart. The damage evolution of the impact fatigue process was monitored in real time by recording the depth change probe depth signal versus time throughout the test. The process is shown in Figure 1(b). The surface position (probe depth) is recorded during the 2 s “on” periods when the probe is in contact with the surface. For the rest of the test the probe is either at the solenoid position or accelerating towards or away from the sample surface. The top-views of the impact craters were observed by high resolution SEM imaging (XL-30 FEI Co., USA).

3. Results and discussion

3.1. Single nano-impact tests

3.1.1 Contact process and analysis parameters of single nano-impact

By performing single nano-impact tests with ‘Dynamic Hardness’ mode, an instantaneous change of probe displacement as a function of impact time can be recorded by using a high data acquisition rate system (Fig 2a). The detailed impact process has been described in Reference [30]. When the solenoid on the bottom of pendulum is released, the indenter tip will accelerate towards the surface of the sample driven by the applied load. In this stage, the velocity of indenter will increase gradually, resulting in increasing kinetic energy. Subsequently, the tip will penetrate into the sample until the velocity decreases to zero, corresponding to the indentation stage in the inset of Fig 2a. During this process, the kinetic energy is transferred into the reversible elastic work, irreversible plastic work and other dissipation processes such as heat loss and frictional work. Subsequently, the stored elastic energy is released, leading to the rebound of the tip. The rebound height will depend on the elastoplastic properties of the sample. Then a new contact cycle with much reduced impact distance will begin until the kinetic energy is exhausted after several contact cycles.

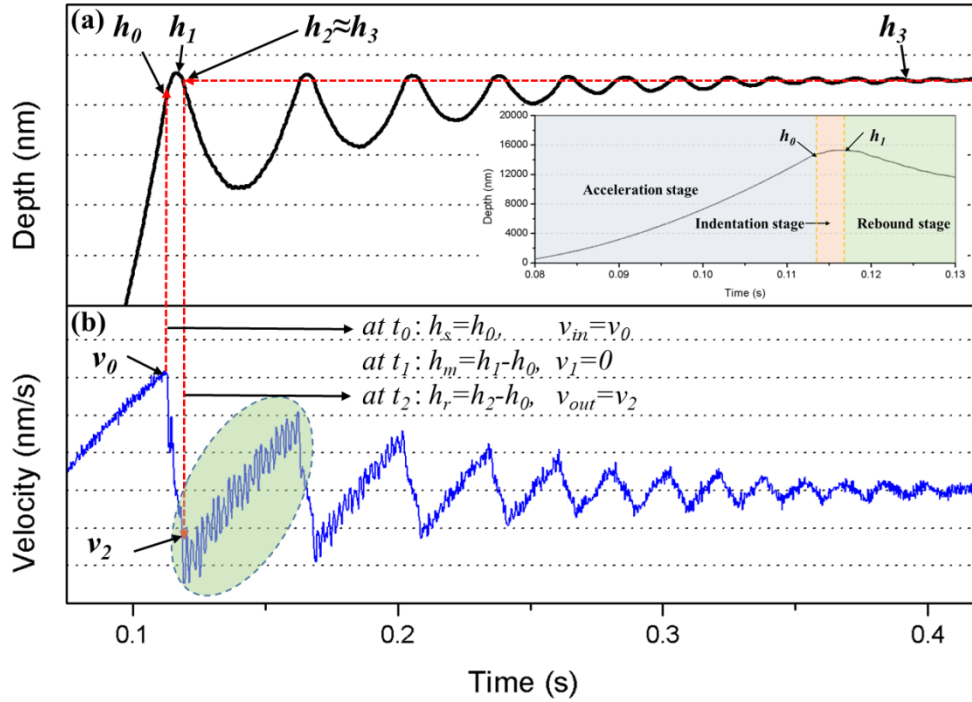


Fig.2 (a) A typical depth vs. time curve of single nano-impact (the insert is the first contact cycle and three different stages), (b) the corresponding velocity vs. time curve.

It is generally assumed that plastic deformation of the material is completed after the first contact cycle, and the parameters like impact depth and velocity before and after the first contact cycle are extracted to calculate the dynamic hardness [10,21,29,33-36]. Nevertheless, there is no standard procedure to determine accurately the depth and velocity information from the single impact curves. As described above, the velocity of indenter tip will reach its peak value when contacting with the sample, so the surface height h_0 can be determined by the fitted and derived maximum velocity ($v_{in} = v_0$) in the acceleration stage (Fig 2b), as has been done in previous studies [10,21,29]. The maximum impact depth h_m can be obtained by the subtracting the surface height h_0 from the maximum height h_1 . The main challenge occurs in how to determine the residual depth h_r and the rebound velocity v_{out} when the indenter detaches from the sample after first contact cycle due to the strong oscillations induced by the reciprocal loading of the compliant (i.e. not infinitely stiff) pendulum, as can be seen in the dotted green ellipse of Fig 2b. To solve this issue, the final rest depth h_3 has been used to approximate the detachment depth h_2 at first contact cycle, and the fitted and derived velocity v_2 at that point of h_2 was regarded as the rebound velocity v_{out} . The difference between the surface height h_0 and the detachment depth h_2 is equal to the residual depth h_r after first contact cycle. This approach appears reasonable and well-founded by Wheeler and co-workers previous study on the influence of rebound impacts [19]. In that study it was found the influence of the rebound impact on the final residual depth can be negligible, as shown by the equivalent residual impression of the single impact and rebound indentations on a copper sample. It is perhaps worth noting that extensive brittle fracture would

necessarily affect this comparison, although over most of the experimental single-impact conditions here it was not observed.

3.1.2 Impact curves and indentation morphology of GLC films

Fig. 3a shows typical impact depth vs. time curves of GLC-2 film deposited on 316L stainless steel under different acceleration loads. As can be seen, each impact curve contains multiple contact cycles, and the maximum contact depth decreases gradually in turn until it comes to rest in a final residual depth, which also confirms the validity of the assumption that the plastic deformation is basically completed in the first contact cycle. The maximum impact depth h_m and the residual depth h_r increase with the acceleration load. It should be noted that the h_r at the lowest impact load of 2 mN is almost zero, indicating the nearly completely elastic deformation of film/substrate system at this load. Fig. 3b compares the typical impact curves of GLC films with different thickness and the uncoated substrate at acceleration load of 10 mN. It can be seen that the GLC film/substrate systems show a lower impact depth than the uncoated substrate.

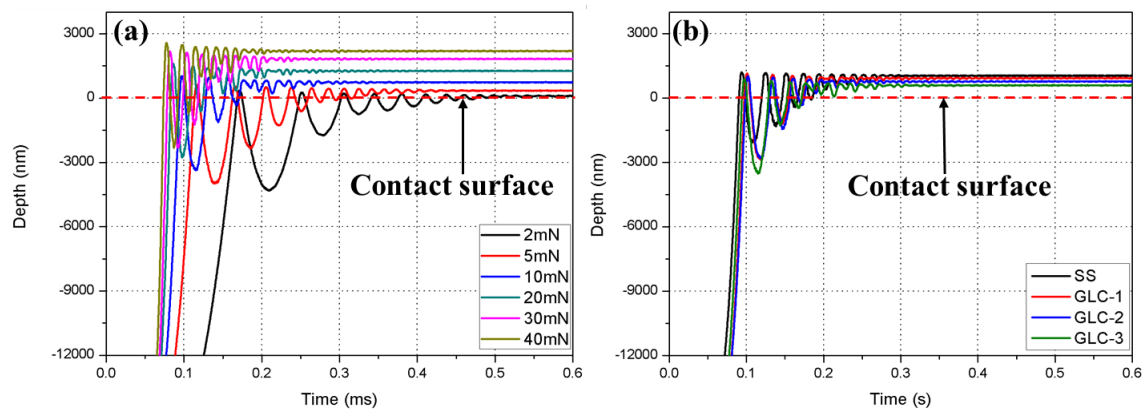


Fig.3 Typical single nano-impact depth-time curves for (a) GLC-2 at different acceleration loads from 2-40 mN, (b) GLC samples with varied thickness and substrate at acceleration load of 10 mN.

For more detailed information, the mean values of h_m , h_r , v_{in} , v_{out} and the ratios of h_r/h_m and v_{out}/v_{in} for different acceleration force were extracted and are shown in Fig. 4. As can be seen from Fig. 4a&b, h_m and h_r of GLC films decrease with increasing film thickness and the values are always lower than the uncoated substrate, which indicates the deposition of the films enhances the impact resistance of the stainless steel substrate and the thicker film provides more load capability for the film/substrate system. To an extent, h_r/h_m reflects the relative elastic and plastic properties of the system. Using three dimensional finite element analysis (FEA) Giannakopoulos and Suresh [37] suggested that h_r/h_m and H/E are linearly related and the h_r/h_m should be basically constant for an elastoplastic material indented with a self-similar indenter. With a spherical indenter the relationship is more complex, but the two properties are still related. As shown in Fig 4c, the h_r/h_m of the substrate material is almost the same

at different acceleration forces, while the value for GLC films is obviously lower at acceleration force of 2 mN and increases gradually to a relatively stable level with increasing acceleration force. This behavior demonstrates that the elastic deformation of hard GLC films play an important role in the film/substrate system at low acceleration force, and as the accelerating force increases there is a transition to deformation dominated by the substrate plasticity. The lower h_r/h_m of GLC-3 is consistent with higher effective (i.e. composite) H/E for the thicker film system. The approximately constant v_{in} for the different samples at a given acceleration force shown in Fig. 4d indicate the very high repeatability of the instrument. The value of v_{out}/v_{in} is usually used to characterize the energy dissipation during impact contact. As shown in Fig. 4f, the thicker film lost less kinetic energy during first contact cycle, attributed to lower plastic deformation.

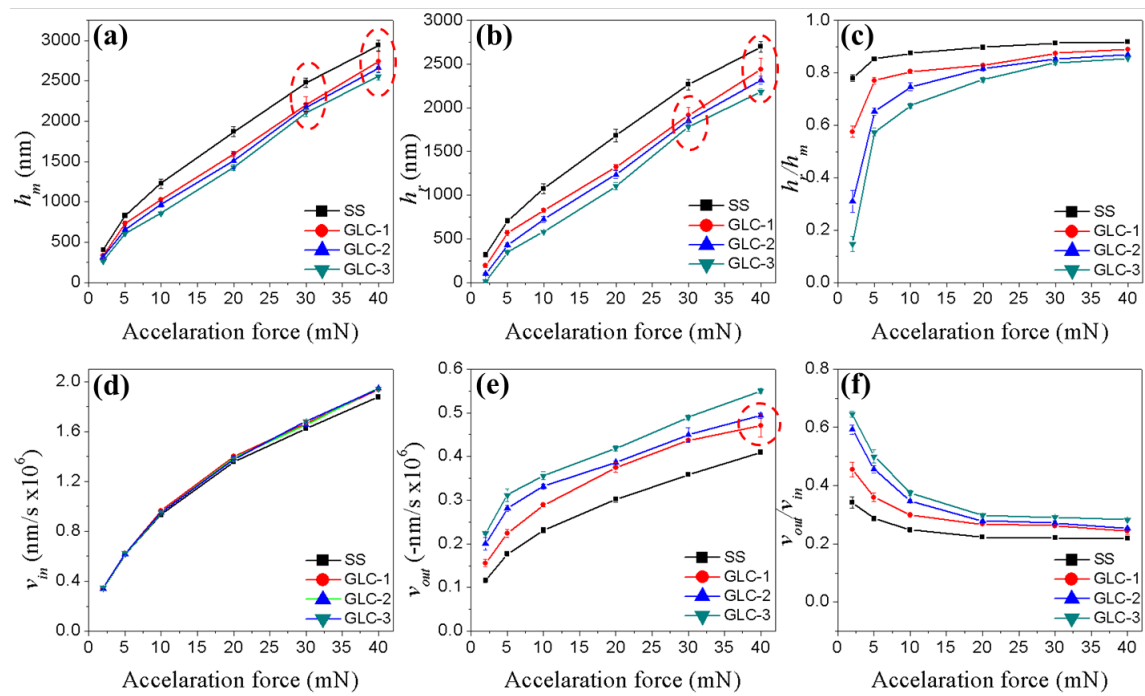


Fig. 4 The variation in the mean values of (a) maximum impact depth (h_m), (b) residual impact depth (h_r), (c) h_r/h_m , (d) contact velocity (v_{in}), (e) rebound velocity (v_{out}), and (f) v_{out}/v_{in} .

Fig. 5 shows AFM images of the typical impact crater morphologies for GLC-3 sample under different acceleration forces. All of the residual impressions show a distinct spherical impact crater shape since the spherical indenter with a diameter of 10 μm is used in this experiment. Both the indentation projected area and residual depth increase with increasing acceleration force, confirming the significant dynamic effect of the nano-impact. No clear circumferential or radial cracks can be identified around the residual impressions for GLC-2 and GLC-3 sample, even at the highest acceleration force. Fig. 5g compares the value of h_r obtained by analysis of impact curves with that measured by AFM topography. This important result shows that the

values obtained by the two methods are basically consistent, providing quantitative validation of the nonlinear fitting derivation method in *Section 3.1.1*. Consequently, the h_r values used in the following calculation are all the results of curve derivation. However, it should be noted in Fig 4a,b and e, the error bar of h_m , h_r and v_{out} for GLC-1 sample at high acceleration force of 30-40 mN is obviously higher than other samples, which could have been caused by crack formation. To test this prediction, the SEM images of surface morphology for GLC-1 after tests at 30 and 40 mN acceleration force are shown in Fig. 6. For this sample clear cohesive failure occurred inside the impact crater at these accelerating forces.

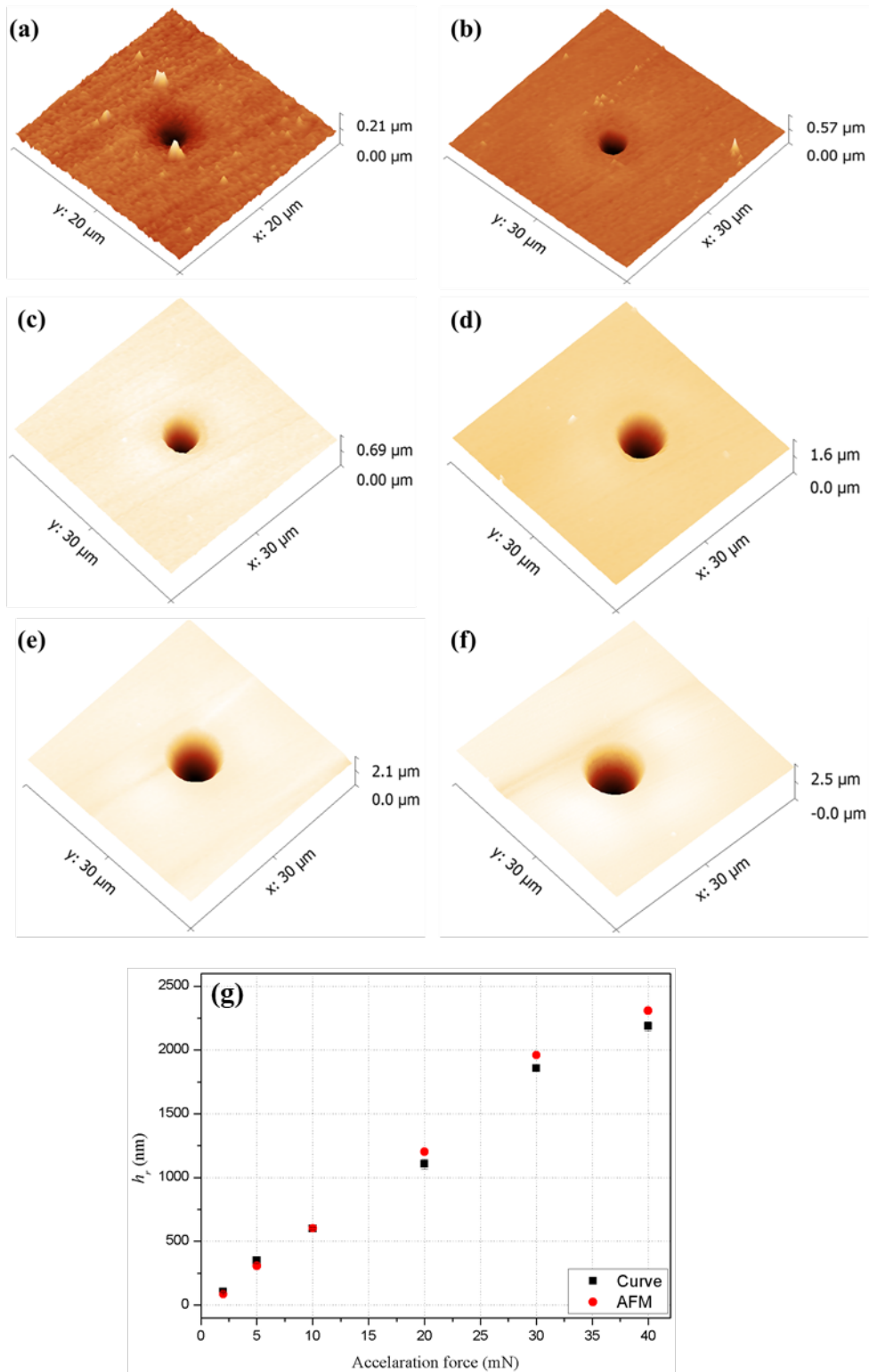


Fig. 5 The typical AFM images of residual impressions for GLC-3 sample at different acceleration forces of (a) 2 mN, (b) 5 mN, (c) 10 mN, (d) 20 mN, (e) 30 mN, (f) 40mN, and (g) the comparison between the value of h_r obtained by analysis of impact curves and that measured by AFM topography.

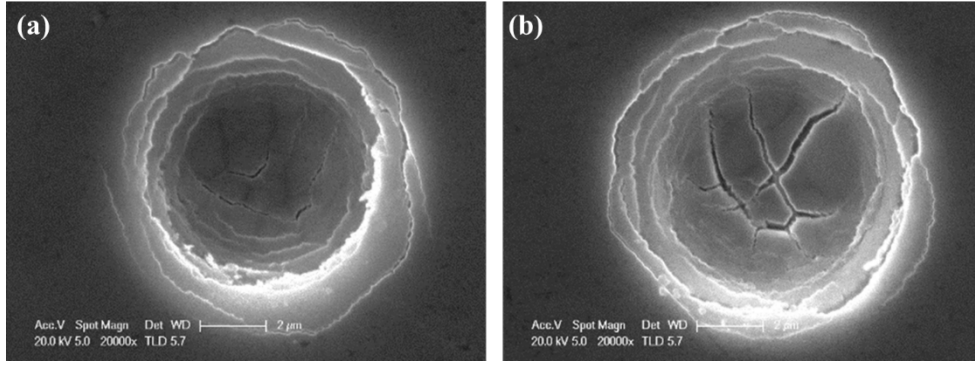


Fig. 6 The SEM images of surface damage on GLC-1 film at acceleration load of (a) 30 mN, (b) 40 mN.

3.1.3 Impact energy and dynamic hardness of GLC films

Similar to the quasi-static hardness (H_s) usually defined as the required force to produce a unit indentation area, the dynamic hardness (H_d) quantifies the absorbed energy per unit volume as the plastic deformation induced by impact response. Based on Tabor's energy approach [38], the equation can be described as:-

$$H_d = \frac{W_p}{V_r} \quad (1)$$

Where V_r is the volume of impact-induced plastic deformation, which can be calculated by Equation (2) due to the spherical morphology shown in Fig. 5:

$$V_r = \frac{\pi}{3} * (3R - h_r) * h_r^2 \quad (2)$$

In which R is the radius of spherical indenter, h_r is residual depth of first impact contact cycle. W_p in Equation (1) is the plastic absorption work, which can be determined from the conversion of kinetic energy before and after the indenter penetrates into the sample. By analyzing the first contact cycle, the total impact energy W_i of the indenter will transformed to the plastic work W_p , the elastic stored work W_e and other energy dissipation W_0 such as the heat loss and friction work. As the impact contact takes place within a very localized area for tens of milliseconds, the W_0 can be neglected [21.36]. W_i and W_e can be calculated by the kinetic energy at contact surface $1/2mv_{in}^2$ and detachment point $1/2mv_{out}^2$, respectively, and m is the effective mass of the pendulum. W_p can therefore be estimated by:-

$$W_p = \frac{1}{2}mv_{in}^2 - \frac{1}{2}mv_{out}^2 \quad (3)$$

Fig. 7 shows the initial contact kinetic energy W_i and the effective acceleration work ratio α (the ratio of W_i and the total work done by acceleration force) at different acceleration forces. The impact energy of the indenter increases linearly with the acceleration force, regardless of the sample or indenter geometry. For acceleration forces of 2-5 mN, the vibration of pendulum and air damping has a significant influence on the movement of indenter, leading to the lower effective acceleration

work ratio α . When the acceleration force increases above 10 mN, the velocity of the indenter reaches a relatively large value, and the energy loss by air damping can be neglected compared to the kinetic energy of the pendulum, generating the near-constant value of the effective acceleration work ratio α shown in the figure.

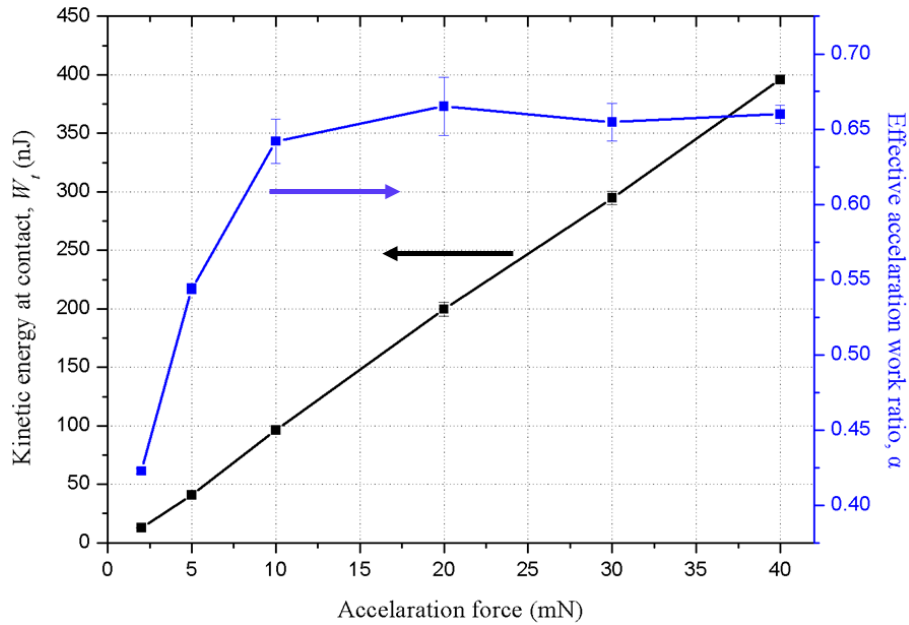


Fig. 7 The initial contact kinetic energy W_i and the effective acceleration work ratio α at different acceleration forces.

To assess the reasonableness and accuracy of the approach for calculating dynamic hardness, it is necessary to compare the results to quasi-static hardness. As can be seen in Fig. 8, the dynamic hardness H_d of GLC films is much larger than that of substrate at low residual depth, and it is closer to the value of substrate material with the increase of residual depth, which is consistent with the quasi-static hardness H_s results shown by the open symbols in Figure 8. This is because the calculated hardness is not the value of only GLC film, but the composite hardness of the film/substrate system. At low acceleration force, the GLC films can provide more load support to the soft substrate, and the intrinsic hardness of the film plays a leading role in the film/substrate system, while the substrate hardness progressively dominates at higher acceleration force. The higher H_d for thicker GLC film at the same residual depth can be attributed to more prominent film effect to resist plastic deformation of the film/substrate system.

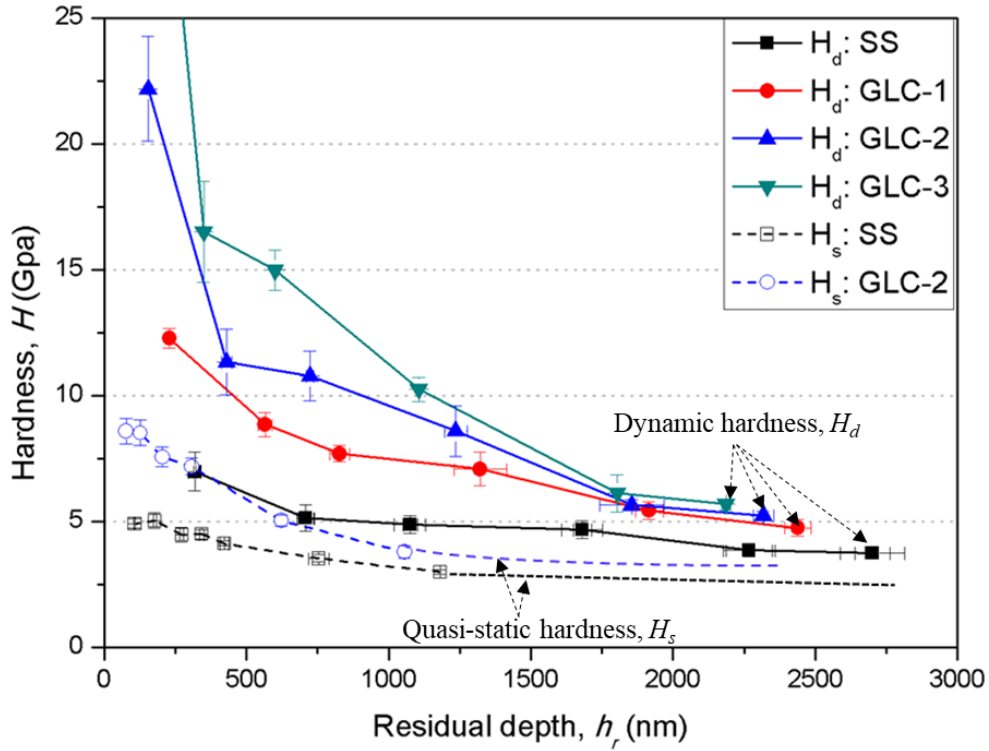


Fig.8 The variation in dynamic hardness and quasi-static hardness for GLC films with varied thickness and uncoated substrate. (Note: partial data on H_s has been published previously in ref. [28])

The indentation size effect (ISE) may also be another important reason for the decreased dynamic hardness with the increased penetration depth, especially for the 316L stainless steel substrate. In general, geometrically necessary dislocation (GND) theories proposed by Nix and Gao have been used to explain the decreasing trend of quasi-static hardness with depth in bulk materials, in which the higher density of GND at small depth leads to the higher hardness [39]. Arreguin-Zavala et al. [40] found the linear strain gradient model is not directly applicable at high strain rate by using the nano-impact technique to investigate dynamic hardness of ultrafine-grain aluminum-silicon claddings. Based on this work, Ghosh et al. [20] further investigated the ISE in nano-impact indentation by analyzing the plastic wave, impact energy and the induced indentation strain. It was suggested the nonuniformity of strain rate promotes the heterogeneity, instability, and localization of strain during nano-impact indentation, resulting in the deviation of H_d from the strain gradient model [41]. As was reported in our previous study[30], the instantaneous strain rate ISR at contact surface is high, $> 10^4 \text{ s}^{-1}$, but rapidly decreases when the indenter penetrates into the sample. The high span and nonuniform strain rate during nano-impact cycle can generate significant strain concentration and enhanced dynamic ISE.

It can be observed in Fig. 8 that the calculated H_d is higher than H_s at the same residual depth for both GLC films and stainless steel substrate, especially at low acceleration force. Firstly, it should be attributed to the overestimation of the energy

absorbed by plastic deformation (W_p) in the calculation of dynamic hardness. As described above, the dissipated energy W_0 is neglected in Equation (3), which includes the adiabatic heating of the sample, friction loss of the indenter, and the absorbed energy of dynamic compliance of the pendulum [19,33]. This part of energy takes up a large proportion of the total kinetic energy at low acceleration, leading to the very high H_d calculated by energy-based method. With the increase of acceleration force, the influence of W_0 is asymptotically decreased, but there is still an effect on the accuracy of H_d . For the thicker GLC films, the higher composite hardness at low acceleration force perhaps causes more energy absorbed by the elastic deflection of the pendulum, resulting in greater calculation error for H_d . Secondly, the formation of micro-cracks at GLC films may also absorb partial energy, and the proportion increases with the increasing of acceleration force, which can be evidenced by the macro-cracks shown in Fig. 6. Finally, the high H_d under dynamic condition may also be caused by high strain rate of nano-impact tests as reported in previous studies [19,21,29]. The dynamic hardness of gold obtained by Constantinides et al. by using nano-impact was higher than the quasi-static hardness due to the rate-dependent energy absorption [21]. Somekawa and Schuh reported the dynamic hardness of fine-grained magnesium alloys is linear with the quasi-static hardness spanning a wide range of strain rates from 10^{-3} to 150 /s [29]. Wheeler et al. [19] also found the dynamic hardness of Cu sample is higher than that at quasi-static condition, particularly clear at shallower impact depth. By comparing the strain rate sensitivity exponent with the value reported in literature, it was suggested that the dynamic hardness obtained from nano-impact indentation is reasonable.

From the above, the dynamic hardness of film/substrate system or films with high thickness at high strain rate can be obtained reasonably by using single nano-impact technology, but the impact energy should be controlled in a suitable range to avoid the high calculation error at low impact energy and the fracture of films at high impact energy. To calculate the exact value of dynamic hardness, further work should be done to extract the dissipated energy W_0 .

3.2. Multiple micro-impact tests

3.2.1 The multiple impulse curves and residual impressions of GLC films

In the ‘Multiple Impulse’ mode, a preset number of impacts with the same initial kinetic energy are performed to strike the same site on the surface of the material repeatedly, and the evolution of impact depth as the function of the impact cycles is recorded, instead of the detailed information of the single impact curve described in the previous section. Fig. 9 a&b shows the 3D surface map (impact cycles-acceleration forces-depth) of GLC-1 and 2D plot (impact depth vs. cycles) of GLC-3 at different acceleration forces, respectively. Multiple impact curves for all of the three GLC samples show similar behavior, where the impact depth increases rapidly at the first few impact cycles, and then increases more slowly to reach an approximately constant plateau depth. The plateau depth and the required impact

number to reach this platform increases with the increasing of acceleration forces. Compared to the rebounding of ‘Dynamic Hardness’ mode, the subsequent impact in ‘Multiple Impulse’ curves possess more energy to generate further plastic deformation, represented by the increasing impact depth. When the impact cycles reach a certain number, the influence of plastic indentation on the total kinetic energy becomes minimal, corresponding to the onset of near-constant impact depth until the end of the test. For a brittle material, another common behavior is a sudden increase of impact depth that signifies the onset of dramatic fracture and material removal. Clearly, this is not the case in this study.

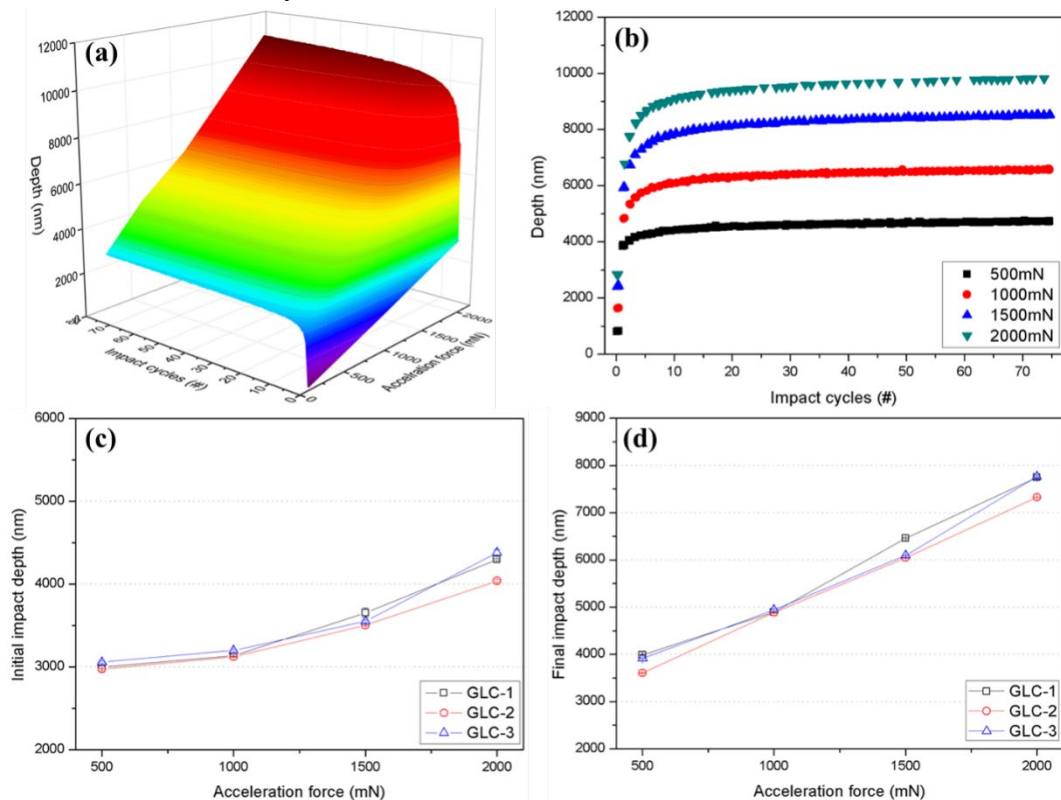


Fig. 9 (a) The 3D surface map (impact cycles-acceleration forces-depth) of GLC-1, (b) 2D plot (impact depth vs. cycles) of GLC-3 at different acceleration forces, (c) the initial impact depth, and (d) the final impact depth for GLC samples with varied thickness at different acceleration forces by multiple micro-impact tests.

Another interesting phenomenon can be observed from the mean initial impact depth and the depth at the end of 75 impact cycles shown in Fig. 9c&d. According to the calculated H_d in Section 3.1.3, the impact depth reported here should decrease with the increase of film thickness. It can be seen the impact depth of GLC-2 is indeed lower than that of GLC-1, but the GLC-3 shows a higher impact depth than GLC-2, indicative of some fracture in the GLC films. The difference in impact depth of GLC films is consistent with the SEM images of the residual damage morphology shown in Fig. 10. For all of the GLC samples, both circumferential cracks and radial cracks are clearly visible at the contact edge and the inner zone of the impact impression, respectively, and the contact damage becomes more and more drastic with the

acceleration force increase from 500 mN to 2000 mN. Nevertheless, no delamination is found around the impact indenter, consistent with the gradually increasing impact depth in Fig. 9b. Besides, it can be observed in Fig. 10 that the cracks under the indenter seem to be dominated in the thinnest GLC-1 film, while the circumferential cracks are more pronounced in the thicker GLC films. For a general comparison, GLC-2 presents the lightest contact damage under multiple micro-impact testing, which is consistent with the mean impact depth in Fig. 9c & d.

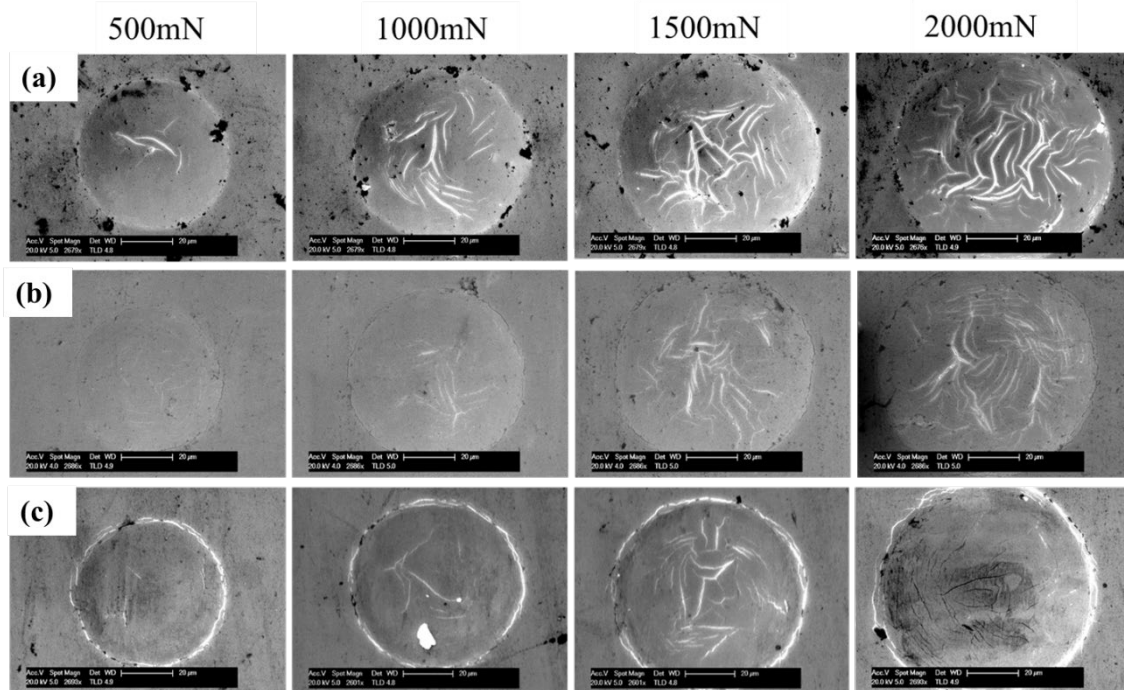


Fig. 10 Typical SEM images of the residual morphology for (a) GLC-1, (b) GLC-2, (c) GLC-3 with different acceleration forces by using multiple micro-impact tests.

3.2.2 Deformation and failure mechanism of GLC films

The deformation and damage of hard thin films under surface contact is closely related to indenter geometry, coating thickness and the elastoplastic properties of films and substrates. For a brittle thin film coated on ductile substrate, the general deformation-damage evolution to repetitive impact contact can be summarized by three stages: (1) plastic deformation of the substrate with possible nucleation of micro-cracks in the thin films, (2) suppression of plastic deformation and the further growth of sub-surface cracks, (3) crack coalescence and fracture in the thin films. This type of contact damage has been reported on DLC films, ceramic coating and amorphous TiNi film by using nano-impact and macro-impact tests [10,22,25]. The mechanism under micro-impact in this research appears to have similar features despite the absence of a rapid change in probe depth shown in Fig. 9b. Gradually increasing depth with the absence of any abrupt depth increases was also observed on continued micro-impact of a crack-resistant amorphous carbon film (Graphit-iC) deposited on a hardened M42 tool steel in our previous study [27], in which the mean contact pressure during micro-impact tests was calculated by Hertzian analysis and

shown a gradual downward trend with each subsequent impact until to the plateau depth. The abrupt increases in depth commonly observed in micro-impact tests on coated systems with higher load supporting substrates (e.g. hardened steels or WC-Co) typically correspond to lateral fractures and material removal. In contrast, with the ductile, soft steel substrate in the current study, the cracking occurs alongside continued substrate plasticity and does not result in lateral fractures.

The fracture mode of brittle coatings on compliant substrates has been investigated by using FEA and indentation experiments. In general, there are three types of crack within the hard thin film under contact load, i.e. radial cracks, ring cracks, and lateral cracks. Radial cracks are usually caused by the radial tensile stress at the film/substrate interface and propagate towards to the surface of films, while the ring crack is dependent on the radial stress at the periphery of the indenter and grow downward to the interior of the films [42,43]. Studies have shown that the location of the maximum stress during loading is influenced by the ratio of contact radius (a) and coating thickness (t), respectively. The high a/t for thin films will generate high tensile stress near the interface center of the film and substrate, while the ring cracks at the edge of the indent are dominant for the low ratios in thick films. For example, Chai and Lawn [44] used FEA to show that there is a transition of fracture mode for the ceramic/polymer bilayer systems indented with a spherical indenter. When the coating is thick enough, the fracture appears as ring cracking around the contact on the top surface. As the coating thickness reduces, the fracture mode first transitions to radial cracking at the interface between the coating and substrate, and finally back to surface ring cracking when the coating thickness drops to an extremely low value. Based on simulation and experimental results of DLC films on Ti substrate, Bernoulli et al. [45] also found the thin DLC films show significant cracking in the inner zone of the indent, while the edge cracking is more distinct for thicker DLC films. SEM images in Fig. 10 shows that for these films the cracks appear to show a similar evolution trend as the value of a/R decreases from 0.039 to 0.013.

Besides the stress distribution, the difference in fracture mode for GLC films with thickness is also attributed to their microstructure and mechanical properties. As reported in our previous study [31], the GLC-1 film has higher intrinsic hardness and H/E , which results in the minimum service life under high load fretting wear tests despite of the reduction of friction coefficient. Similarly, the GLC-1 film also shows more severe contact damage under micro-impact tests. For GLC-1 film, the higher intrinsic hardness will aggravate the mismatch of plastic deformation between the film and substrate during unloading process, resulting in the film being more susceptible to radial cracking in micro-impact tests. The thicker GLC films provide more load support and help to reduce the extent of plastic deformation of the substrate, which may eventually increase the possibility of ring cracks around the indenter, and reduce the occurrence of radial cracking. The microstructure is looser and more defects are observed in the surface and cross-sectional SEM images of thicker GLC films in

Reference [31]. The presence of defects will generate uncertainty in crack location and aggravate the occurrence of cracks. Bernoulli et al. [45] proposed that the probability to initial first failure at the edge or at the interface center is nearly identical for the defect-controlled cracking in DLC films with thickness between 900 nm and 1.6 μm , depending on the position and size of the defect.

Compressive residual stress in the films also has an influence on the initiation of cracks. Abdul-Baqi and Van der Giessen [46] simulated a great range of residual stresses from -10 GPa to 10 GPa to investigate the effect of residual stresses on delamination of strong film/ductile substrate system. It was found the delamination can be delayed by compressive stress, while the tensile stress shows the opposite result. Singh et al. [42] also found the compressive residual stress can counteract the radial tensile stress at the surface and base of DLC films, thus impeding the formation of radial and ring cracks. By measuring the curvature radius of Si substrate before and after depositing GLC films, the obtained compressive internal stress for GLC films in this research increases from 0.32 GPa to 1.02 GPa with the increase of film thickness [31]. The high compressive stress for GLC-3 partially offsets the tensile stresses generated by micro-impact, reducing probability of radial and ring cracks forming on the surface of GLC film.

4. Conclusion

In this paper, the dynamic contact behavior of GLC films with varied thickness, 0.55-1.52 μm , was investigated systematically by using the single nano-impact and new-developed repetitive micro-impact testing, respectively. Through the energy-based method, the dynamic hardness of GLC film/substrate system was calculated reasonably by extracting the depth and velocity information of the indenter from the single nano-impact curves. The results show higher dynamic hardness than the quasi-static hardness. This may be attributed to the neglecting of dissipated energy W_0 and strain rate sensitivity of substrate material in the energy-based method. The thickest film can provide more load capability for the substrate, shown as higher composite H_d of film/substrate system.

In the multiple micro-impact tests, the observed fracture behavior was sensitive to the coating thickness. The thinnest film has higher sensitivity to radial cracks in the inner zone of the indent, despite its higher intrinsic hardness. In contrast the thickest GLC film provided more load capability, but more pronounced ring cracks at the edge of the impact crater caused by more defects and looser microstructure. The medium thickness film seems to display the best impact fatigue resistance due to the combined effects of stress distribution, microstructure and mechanical properties. This study provides a rapid method to evaluate the dynamic mechanical properties and fatigue resistance of hard films on ductile substrates experiencing high-load repeated contact, which is very important in the optimization of film thickness to prolong the service

life of components.

5. Acknowledgments

The authors gratefully acknowledge the financial support from the Fundamental Research Funds for the Central Universities, China (Grant No: B200201068, B200205011), the National Natural Science Foundation of China (#11472080), and the funding from Innovate UK Project No: 132369 – “Nano-to Micro-Impact Testing: An in-situ test for UK SEAC sector”.

Declaration of Competing Interest

There are no conflicts to declare.

References:

- [1]K. Bewilogua, D. Hofmann, History of diamond-like carbon films — From first experiments to worldwide applications, *Surface and Coatings Technology*, 242(2014) 214-225.
- [2]R. Hauert, DLC films in biomedical applications, 2008.
- [3]J. Robertson, Diamond-like amorphous carbon, *Materials Science & Engineering R Reports*, 37(2002) 129-281.
- [4]Y. Wang, J. Li, L. Shan, J. Chen, Q. Xue, Tribological performances of the graphite-like carbon films deposited with different target powers in ambient air and distilled water, *Tribology International*, 73(2014) 17-24.
- [5]D. Dong, B. Jiang, H. Li, Y. Du, C. Yang, Effect of graphite target power density on tribological properties of graphite-like carbon films, *Applied Surface Science*, 439(2018) 900-909.
- [6]D. Bernoulli, A. Wyss, R. Raghavan, K. Thorwarth, R. Hauert, R. Spolenak, Contact damage of hard and brittle thin films on ductile metallic substrates: an analysis of diamond-like carbon on titanium substrates, *Journal of Materials Science*, 50(2015) 2779-2787.
- [7]D. Du, D. Liu, Z. Ye, X. Zhang, F. Li, Z. Zhou, L. Yu, Fretting wear and fretting fatigue behaviors of diamond-like carbon and graphite-like carbon films deposited on Ti-6Al-4V alloy, *Applied Surface Science*, 313(2014) 462-469.
- [8]L. Ji, H. Li, F. Zhao, W. Quan, J. Chen, H. Zhou, Effects of environmental molecular characteristics and gas - surface interaction on friction behaviour of diamond-like carbon films, *Journal of Physics D: Applied Physics*, 42(2009) 135301.
- [9]S.K. Field, M. Jarratt, D.G. Teer, Tribological properties of graphite-like and diamond-like carbon coatings, *Tribology International*, 37(2004) 949-956.
- [10]J.M. Wheeler, A.G. Gunner, Analysis of failure modes under nano-impact fatigue of coatings via high-speed sampling, *Surface and Coatings Technology*, 232(2013) 264-268.
- [11]S. Lamri, C. Langlade, G. Kermouche, Damage phenomena of thin hard coatings submitted to repeated impacts: Influence of the substrate and film properties, *Materials Science & Engineering A*, 560(2013) 296-305.
- [12]L. J., Zhu, H. M., Leyland, Mththews, Impact wear and abrasion resistance of CrN, AlCrN and AlTiN PVD coatings, *Surface and Coatings Technology*, 215(2013) 170-177.
- [13]Z. Fan, Y. Liu, S. Xue, R.M. Rahimi, D.F. Bahr, H. Wang, X. Zhang, Layer thickness dependent

- strain rate sensitivity of Cu/amorphous CuNb multilayer, *Applied Physics Letters*, 110(2017) 161905.
- [14]K.D. Bouzakis, S. Gerardis, G. Skordaris, E. Bouzakis, Nano-impact test on a TiAlN PVD coating and correlation between experimental and FEM results, *Surface and Coatings Technology*, 206(2011) 1936-1940.
- [15]J. Liu, B. Xu, H. Wang, X. Cui, G. Jin, Z. Xing, E. Liu, Investigations on fatigue behavior and surface damage of Cu film by nano impact and molecular dynamics simulation, *Surface and Coatings Technology*, 364(2019) 204-210.
- [16]M. Rueda-Ruiz, B.D. Beake, J.M. Molina-Aldareguia, New instrumentation and analysis methodology for nano-impact testing, *Materials & Design*, 192(2020) 108715.
- [17]S.J. McMaster, T.W. Liskiewicz, A. Neville, B.D. Beake, Probing fatigue resistance in multi-layer DLC coatings by micro- and nano-impact: Correlation to erosion tests, *Surface and Coatings Technology*, 402(2020) 126319.
- [18]E. Frutos, J.L. González-Carrasco, T. Polcar, Repetitive nano-impact tests as a new tool to measure fracture toughness in brittle materials, *Journal of the European Ceramic Society*, 36(2016) 3235-3243.
- [19]J.M. Wheeler, J. Dean, T.W. Clyne, Nano-impact indentation for high strain rate testing: The influence of rebound impacts, *Extreme Mechanics Letters*, 26(2019) 35-39.
- [20]A. Ghosh, S. Jin, J. Arreguin-Zavala, M. Brochu, Characterization and investigation of size effect in nano-impact indentations performed using cube-corner indenter tip, *Journal of Materials Research* 32(2017) 2241-2248.
- [21]G. Constantinides, C.A. Tweedie, N. Savva, J.F. Smith, K.J. Van Vliet, Quantitative Impact Testing of Energy Dissipation at Surfaces, *Experimental Mechanics*, 49(2009) 511-522.
- [22]N.H. Faisal, R. Ahmed, R. Fu, Nano-impact (fatigue) characterization of as-deposited amorphous nitinol thin film, *Coatings*, 2(2012) 195-209.
- [23]N.H. Faisal, R. Ahmed, Y.Q. Fu, Y.O. Elakwah, M. Alhoshan, Influence of indenter shape on DLC film failure during multiple load cycle nanoindentation, *Materials Science & Technology*, 28(2012) 1186-1197.
- [24]B.D. Beake, S.R. Goodes, J.F. Smith, R. Madani, C.A. Rego, R.I. Cherry, T. Wagner, Investigating the fracture resistance and adhesion of DLC films with micro-impact testing, *Diamond & Related Materials*, 11(2002) 1606-1609.
- [25]B.D. Beake, S.P. Lau, J.F. Smith, Evaluating the fracture properties and fatigue wear of tetrahedral amorphous carbon films on silicon by nano-impact testing, *Surface and Coatings Technology*, 177-178(2004) 611-615.
- [26]J. Chen, R. Ji, R.H.U. Khan, X. Li, B.D. Beake, H. Dong, Effects of mechanical properties and layer structure on the cyclic dynamic loading of TiN-based coatings, *Surface and Coatings Technology*, 206(2011) 522-529.
- [27]B.D. Beake, T.W. Liskiewicz, A. Bird, X. Shi, Micro-scale impact testing - A new approach to studying fatigue resistance in hard carbon coatings, *Tribology International*, 149(2020) 105732.
- [28]E.W. Andrews, A.E. Giannakopoulos, E. Plisson, S. Suresh, Analysis of the impact of a sharp indenter, *International Journal of Solids and Structures*, 39(2002) 281-295.
- [29]H. Somekawa, C.A. Schuh, High-strain-rate nanoindentation behavior of fine-grained magnesium alloys, *Journal of Materials Research*, 27(2012) 1295-1302.
- [30]L. Qin, H. Li, X. Shi, B.D. Beake, L. Xiao, J.F. Smith, Z. Sun, J. Chen, Investigation on dynamic

- hardness and high strain rate indentation size effects in aluminium (110) using nano-impact, *Mechanics of Materials*, 133(2019) 55-62.
- [31]X. Shi, T.W. Liskiewicz, B.D. Beake, J. Chen, C. Wang, Tribological performance of graphite-like carbon films with varied thickness, *Tribology International*, 149(2020) 105586.
- [32]A.C. Fischer-Cripps, *Nanoindentation Test Standards*, Springer New York, 2011.
- [33]N.M. Jennett, J. Nunn, High resolution measurement of dynamic (nano) indentation impact energy: a step towards the determination of indentation fracture resistance, *Philosophical Magazine*, 91(2011) 1200-1220.
- [34]H. Somekawa, C.A. Schuh, Nanoindentation behavior and deformed microstructures in coarse-grained magnesium alloys, *Scripta Materialia*, 68(2013) 416-419.
- [35]J.R. Trelewicz, C.A. Schuh, The Hall - Petch breakdown at high strain rates: Optimizing nanocrystalline grain size for impact applications, *Applied Physics Letters*, 93(2008) 171916.
- [36]C. Zehnder, J. Peltzer, J.S.K.L. Gibson, S. Korte-Kerzel, High strain rate testing at the nano-scale: A proposed methodology for impact nanoindentation, *Materials & Design*, 151(2018) 17-28.
- [37]A.E. Giannakopoulos, S. Suresh, Determination of elastoplastic properties by instrumented sharp indentation, *Scripta Materialia*, 40(1999) 1191-1198.
- [38]D. Tabor, A simple theory of static and dynamic hardness, *Proceedings of the Royal Society of London. Series A: Mathematical and Physical Sciences*, 192(1948) 247-274.
- [39]W.D. Nix, H.J. Gao, Indentation size effects in crystalline materials: A law for strain gradient plasticity, *Journal of the Mechanics and Physics of Solids*, 46(1998) 411-425.
- [40]J. Arreguin-Zavala, J. Milligan, M.I. Davies, S.R. Goodes, M. Brochu, Characterization of Nanostructured and Ultrafine-Grain Aluminum-Silicon Claddings using the Nanoimpact Indentation Technique, *JOM-US*, 65(2013) 763-768.
- [41]C. Zener, J.H. Hollomon, Effect of Strain Rate Upon Plastic Flow of Steel, *Journal of Applied Physics*, 15(1944) 22-32.
- [42]R.K. Singh, M.T. Tilbrook, Z.H. Xie, A. Bendavid, P.J. Martin, P. Munroe, M. Hoffman, Contact damage evolution in diamondlike carbon coatings on ductile substrates, *Journal of Materials Research*, 23(2008) 27-36.
- [43]Z.H. Xie, R. Singh, A. Bendavid, P.J. Martin, P.R. Munroe, M. Hoffman, Contact damage evolution in a diamond-like carbon (DLC) coating on a stainless steel substrate, *Thin Solid Films*, 515(2007) 3196-3201.
- [44]H. Chai, B.R. Lawn, Fracture mode transitions in brittle coatings on compliant substrates as a function of thickness, *Journal of Materials Research*, 19(2004) 1752-1761.
- [45]D. Bernoulli, A. Wyss, R. Raghavan, K. Thorwarth, R. Hauert, R. Spolenak, Contact damage of hard and brittle thin films on ductile metallic substrates: an analysis of diamond-like carbon on titanium substrates, *Journal of Materials Science*, 50(2015) 2779-2787.
- [46]A. Abdul-Baqi, E. Van der Giessen, Delamination of a strong film from a ductile substrate during indentation unloading, *Journal of Materials Research*, 16(2001) 1396-1407.